⌘ *Author's Choice*

THE JOURNAL OF BIOLOGICAL CHEMISTRY VOL. 286, NO. 4, pp. 2946–2955, January 28, 2011

Human Perforin Employs Different Avenues to Damage Membranes*[S]

Received for publication, July 28, 2010, and in revised form, September 27, 2010 Published, JBC Papers in Press, October 2, 2010, DOI 10.1074/jbc.M110.169417

Tilen Praper[‡1–3], Andreas Sonnen[§3,4], Gabriella Viero[¶5], Aleš Kladnik[‡], Christopher J. Froelich[‖], Gregor Anderluh[‡2,6,7], Mauro Dalla Serra[¶8], and Robert J. C. Gilbert[§6,9]

From the [‡]Department of Biology, Biotechnical Faculty, University of Ljubljana, Večna pot 111, 1000 Ljubljana, Slovenia, the [§]Division of Structural Biology, Wellcome Trust Centre for Human Genetics, Oxford OX3 7BN, United Kingdom, the [¶]National Research Council, Institute of Biophysics and Bruno Kessler Foundation, via alla Cascata 56/C, 38123 Trento, Povo, Italy, and the [‖]Department of Medicine, NorthShore University HealthSystem Research Institute, Evanston, Illinois 60201

Perforin (PFN) is a pore-forming protein produced by cytotoxic lymphocytes that aids in the clearance of tumor or virus-infected cells by a mechanism that involves the formation of transmembrane pores. The properties of PFN pores and the mechanism of their assembly remain unclear. Here, we studied pore characteristics by functional and structural methods to show that perforin forms pores more heterogeneous than anticipated. Planar lipid bilayer experiments indicate that perforin pores exhibit a broad range of conductances, from 0.15 to 21 nanosiemens. In comparison with large pores that possessed low noise and remained stably open, small pores exhibited high noise and were very unstable. Furthermore, the opening step and the pore size were dependent on the lipid composition of the membrane. The heterogeneity in pore sizes was confirmed with cryo-electron microscopy and showed a range of sizes matching that observed in the conductance measurements. Furthermore, two different membrane-bound PFN conformations were observed, interpreted as pre-pore and pore states of the protein. The results collectively indicate that PFN forms heterogeneous pores through a multistep mechanism and provide a new paradigm for understanding the range of different effects of PFN and related membrane attack complex/perforin domain proteins observed *in vivo* and *in vitro*.

Cytotoxic T lymphocytes and natural killer cells provide an essential line of defense by eliminating pathogen-infected and tumor cells through a process called granule-mediated apoptosis. This phenomenon involves the secretion of PFN[10] postulated to aid the intracellular delivery of granule-associated proteases (granzymes) resulting in the death of the target cell (1–3). How this delivery is achieved is subject to intense debate. Broadly, there are two alternative models as follows: either PFN forms pores at the cell membrane through which granzymes are delivered directly or PFN forms pores in endosomes containing granzymes and thereby delivers them to the cytosol (1–3). Nevertheless, the ability of PFN to perforate the target membranes by transmembrane pores is central to each model (1–3).

PFN is a multidomain protein. The largest portion, including around two-thirds of the molecule starting from the N terminus, is the membrane attack complex/perforin (MACPF) domain (1–2). PFN also contains an epidermal growth factor-like domain (EGF) of an unknown function and a C2 domain at the C terminus, which is needed for calcium-dependent binding to lipid membranes (supplemental Fig. 1, *A* and *B*) (4, 5). The structure of the MACPF domain is strikingly similar to the pore-forming domain of the cholesterol-dependent cytolysin (CDC) protein family from Gram-positive bacteria, and it is therefore believed that both protein families use a similar mechanism for transmembrane pore formation (6–8). CDCs are important pathogenicity factors, and prominent members of the family include pneumolysin from *Streptococcus pneumoniae*, perfringolysin (*Clostridium perfringens*), streptolysin (*S. pneumoniae*), and listeriolysin (*Listeria monocytogenes*) (9, 10). CDCs form pores by inserting a huge β-barrel across the membrane, each monomer contributing two transmembrane β-hairpins that refold from six α-helices within domain 3 (supplemental Fig. 1, *C–E*) (10). These crucial structural elements are conserved between CDC and MACPF domains and are deployed after oligomerization (7, 10). Baran *et al.* (11) have described two amino acid residues

* This work was supported, in whole or in part, by National Institutes of Health Grant 5RO1AI04494-03. This work was also supported in part by a Slovenian-Italian collaborative grant.

⌘ *Author's Choice*—Final version full access.

[S] The on-line version of this article (available at http://www.jbc.org) contains supplemental Figs. S1 and S2 and additional references.

[1] Supported by the FEBS Collaborative Experimental Scholarship for Central and Eastern Europe and by the Slovene Human Resources Development and Scholarship fund.

[2] Supported by Slovenian Research Agency.

[3] Both authors contributed equally to this work.

[4] Recipient of a Wellcome Trust 4-year Ph.D. Studentship in Structural Biology.

[5] Present address: Laboratory of Translational Genomics, Centre for Integrative Biology, University of Trento, via delle Regole 101, 38060 Mattarello (TN), Italy.

[6] Supported in part by the award of a Royal Society International Joint Project grant and EMBO short term fellowship.

[7] To whom correspondence may be addressed. Tel.: 386-14233388; Fax: 386-12573390; E-mail: gregor.anderluh@bf.uni-lj.si.

[8] To whom correspondence may be addressed. Tel.: 39-0461-314156; Fax: 39-0461314875; E-mail: mauro.dallaserra@cnr.it.

[9] Royal Society University Research Fellow. To whom correspondence may be addressed. Tel.: 44-1865-287535; Fax: 44-1865-287547; E-mail: gilbert@strubi.ox.ac.uk.

[10] The abbreviations used are: PFN, perforin; MACPF, membrane attack complex/perforin; GUV, giant unilamellar vesicle; LUV, large unilamellar vesicle; CDC, cholesterol-dependent cytolysin; CHO, cholesterol; DOPC, 1,2-dioleoyl-*sn*-glycero-3-phosphocholine; rDHPE, rhodamine B 1,2-dihexadecanoyl-*sn*-glycero-3-phosphoethanolamine; DPhPC, 1,2-diphytanoyl-*sn*-glycero-3-phosphocholine; S, siemens; PLM, planar lipid membrane; POPC, 1-palmitoyl-2-oleoyl-*sn*-glycero-3-phosphocholine.

that participate in oligomerization of monomers after PFN binds to the membrane. It has been conclusively shown that CDCs form pores by a two-stage mechanism. First, the protein oligomerizes into a pre-pore state; second, a pore forms (10, 12). There is good evidence that pre-pores and pores can be either complete ring-shaped oligomers or incomplete arc-shaped ones (9). The inner diameter of the PFN pore was determined to be 7–16 nm when measured by the electron microscopy (13, 14), and incomplete rings (so-called arcs) were observed adjacent to completely oligomerized PFN pores (rings) (15–17). Because the inner pore diameter obtained by photobleaching or electrophysiological methods also ranged from 5 to 10 nm (15, 18–21), the existence of pleomorphic oligomeric states emphasizes that the exact molecular mechanism of PFN pore formation remains poorly understood.

To gain insight into the mechanism of PFN pore formation, we have conducted a detailed study using several model membrane systems, clearly showing that native human PFN forms pores of heterogeneous size. The data are consistent with direct insertion of the full ring-shaped pre-pore complex into the lipid bilayer as a pore, as well as the assembly of a transmembrane pore by oligomerization of monomers to an incompletely formed protein channel (an arc) that can form a pore, on membrane insertion, at a protein-lipid interface. The data convincingly show that pore assembly and insertion into the membrane are modulated by the lipid composition of the membrane and that PFN pores have two very distinctive alternative states, either with noisy or noise-free conductance, and with some pores appearing to expand in size while active. We also image two different oligomeric conformations of membrane-bound PFN, which indicate that it can exist in both pre-pore and pore states, validating a CDC-like two-stage mechanism of membrane interaction.

EXPERIMENTAL PROCEDURES

Materials—Native human PFN was isolated as described by Froelich *et al.* (22). Cholesterol (CHO), 1,2-diphytanoyl-*sn*-glycero-3-phosphocholine (DPhPC), 1,2-dioleoyl-*sn*-glycero-3-phosphocholine (DOPC), and 1-palmitoyl-2-oleoyl-*sn*-glycero-3-phosphocholine (POPC) were from Avanti Polar Lipids (Alabaster, AL). Rhodamine B 1,2-dihexadecanoyl-*sn*-glycero-3-phosphoethanolamine, triethylammonium salt (rDHPE), and dextrans labeled with Alexa Fluor 488 (3 and 10 kDa), rhodamine B (10 kDa), or Oregon Green 488 (70 kDa) were from Invitrogen. Dextrans labeled with fluorescein isothiocyanate (FITC) (4, 10, and 70 kDa) were from Sigma. All other chemicals were from Sigma or Merck, unless stated otherwise.

Electroformation of GUVs—GUVs were prepared by electroformation as described (23) with modifications. The lipids were dissolved in chloroform/methanol (2:1, v/v) to a final 1 mM concentration. 25 μl of the lipid solution was spread onto a pair of platinum electrodes and dried under reduced pressure for 2 h. Electrodes (dimensions: inner diameter 1 mm, length 34 mm, and spacing between electrodes 4 mm) were then placed into a vial filled with sucrose buffer (295 mM sucrose, 1 mM HEPES, 0.25 mM $CaCl_2$). AC current was applied with a functional generator (GW Instek GFG-3015). The protocol for electroformation was as follows: 2 h of 4 V/10 Hz; 15 min of 2 V/5 Hz; 15 min of 1 V/2.5 Hz; 30 min of 1 V/1 Hz. GUVs were sedimented with the glucose buffer (295 mM glucose, 1 mM HEPES, 0.25 mM $CaCl_2$). The buffer was then exchanged by gentle pipetting with 150 mM NaCl, 20 mM HEPES, 0.25 mM $CaCl_2$, pH 7.4. GUVs were then divided into aliquots containing approximately equal amounts of vesicles.

Fluorescence Microscopy—6 μl of GUV suspension was mixed with 0.5 or 1 μl of PFN and 0.5 μl of dextran. Final concentrations were 12 nM (PFN), 0.1 mM (D3 and D4), 0.03 mM (D10), or 0.01 mM (D70). Buffer was used for control experiments instead of PFN. The mixture was then incubated at 25 °C monitoring the permeabilization by fluorescent microscopy. Fluorescence and differential interference contrast microscopy (DIC) was performed on AxioImager Z1 (Carl Zeiss, Germany) equipped with an ApoTome for recording of optical sections (grid-confocal microscopy) and 100-watt HBO mercury arc illumination. FITC-labeled dextrans were observed with 450–490-nm bandpass excitation and 515-nm long pass emission filter. The membranes of the GUV-containing rDHPE were observed with 546/12-nm bandpass excitation and 590-nm long pass emission filter. Kinetics of probe influx were recorded by confocal laser-scanning microscopy on a Leica TCS SP5 laser-scanning microscope, mounted on a Leica DMI 6000 CS inverted microscope (Leica Microsystems, Germany). An HCX plan apo ×63 (numerical aperture, 1.4) oil immersion objective was used. Probes (D3, D10, or D70) were excited with the 488-nm line of the argon laser. Fluorescence emission was detected at 500–530 nm. The rDHPE in the GUV membranes was excited with the 543-nm line of the argon laser. Fluorescence emission was detected at 605–650 nm.

Planar Lipid Bilayer Experiments—Solvent-free PLM were prepared as described by Dalla Serra and Menestrina (24). The 2-ml chambers were made of Teflon. The septum between the chambers was made of 25-μm-thick Teflon film and contained a 180-μm hole. PFN was added at 0.2 to 1.1 nM concentrations to stable preformed bilayers on the *cis* side only (the *cis* side is where the electrical potential was applied, and the *trans* side was grounded). All experiments, except selectivity measurements, were performed in symmetric conditions by using a buffer consisting of 100 mM KCl, 20 mM HEPES, 0.1 mM $CaCl_2$, pH 7.4, on both sides of the membrane. A constant voltage, generally 40 mV, was applied across the membrane. Miniature magnetic stir bars stirred the solutions on both sides of the membrane. The current across the bilayer was measured, and the conductance (G) was determined as shown in Equation 1,

$$G(\text{nS}) = I(\text{pA})/V(\text{mV}) \quad \text{(Eq. 1)}$$

where I is the current through the membrane, and V is the applied transmembrane potential. Ionic currents were recorded by a patch clamp amplifier (Axopatch 200, Axon Instruments, Foster City, CA). A PC equipped with a DigiData 1200 A/D converter (Axon Instruments) was used for data acquisition. The current was filtered at 0.5 kHz and acquired at 2 kHz by the computer using Axioscope 8 software (Axon

Instruments). All measurements were performed at room temperature.

For the selectivity determination, a three times activity gradient of KCl was formed, whereby the higher concentration was on the *trans* side. Reversal voltage (V_{rev}) required to null the transmembrane current was converted into the selectivity index giving the ratio of the permeability of cations over the anions (P_+/P_-) by the standard Goldman-Hodgkin-Katz Equation 2 (24),

$$P_+/P_- = ((a_{trans}/a_{cis}) \cdot \exp(eV_{rev}/kT) - 1)/((a_{trans}/a_{cis}) - \exp(eV_{rev}/kT)) \quad \text{(Eq. 2)}$$

where a_{trans} and a_{cis} are the activities of KCl in *trans* and *cis* side, respectively. kT/e is ~25 mV at room temperature.

The diameters of PFN pores were calculated according to Equation 3,

$$d(\text{nm}) = 2\sqrt{10}((G(\text{nS})1(\text{nm}))/(\sigma(\pi)) \quad \text{(Eq. 3)}$$

where d is the pore diameter; σ is the conductivity of the solution (*e.g.* 11 mS/cm for KCl 0.1 M); l is the length of the pore (estimated to be 20 nm from EM data (16) and estimate from our cryo-EM data), and G is its conductance.

To quantify the noise, we determined the standard deviation of the current on a short time interval (typically ~10 s) for the individual current trace. Standard deviation was then normalized by dividing it with the average current of each trace to obtain normalized noise.

Cryo-EM—400 μl of 10 mg/ml DOPC in chloroform (Avanti Polar Lipids) and 40 μl of 25 mg/ml CHO in chloroform (Avanti Polar Lipids) were dried on a clean Pyrex tube under argon. Residual chloroform was removed by overnight desiccation in a desiccator attached to a VARIO-SP Diaphragm Pump (Vacuubrand, Germany). The lipid film was then hydrated by addition of 1 ml of liposome buffer (20 mM HEPES, 150 mM NaCl, 250 μM $CaCl_2$, pH 7.4) at 50 °C followed by vigorous vortexing, giving an ~5 mg/ml lipid dispersion. After 10 freeze-thaw cycles alternating between liquid nitrogen, a 50 °C water bath and a 1-min vortexing step, the dispersion was extruded 11 times with a Mini Extruder (Avanti Polar Lipids) through a Whatman polycarbonate membrane with a pore diameter of 100 nm. Liposomes were used immediately after preparation. PFN was added to liposomes at a final concentration of 10–20 ng/μl and incubated at either room temperature or 37 °C. If at the latter temperature, then the liposomes and PFN were individually preincubated at 37 °C. Incubation times varied from 5 s to 5 min. The number of pores was accentuated by longer incubations and 37 °C temperature. As a control for the effect of PFN itself, we incubated a mixture of PFN buffer and LUVs at the same ratios used with PFN present. Samples were flash-frozen using liquid ethane on 300 mesh lacey carbon grids and imaged using an FEI F30 FEG cryo-electron microscope operating at liquid nitrogen temperatures. Images were captured on SO-163 film (Kodak) and scanned using a Zeiss SCAI scanner. Micrographs were corrected for their CTF using CTFFIND3 (25) and EMAN (26). Images of pores were individually boxed using the EMAN suite program BOXER and subjected to image alignment and analysis using IMAGIC software (27). Density was visualized using UCSF Chimera (28). The homology model of perforin was calculated using the PHYRE web server (29, 30).

RESULTS

Perforin Forms Heterogeneous Pores on GUVs—GUVs were generated by electroformation from DOPC/CHO/rDHPE at a molar ratio 79:20:1. rDHPE was used to mark the membrane. We have found that such a lipid composition enables stable Ca^{2+}-dependent PFN binding as monitored by surface plasmon resonance in a related LUV system (31). The use of fluorescent microscopy enabled us to monitor the movement of fluorescent dextran molecules co-administered with PFN into the GUVs when at least 100 μM Ca^{2+} was used. In the absence of Ca^{2+}, no permeabilization of GUVs was observed, and spontaneous passage of probes into the GUV in the absence of PFN was negligible (Fig. 1*A*). The presence of PFN at 12 nM final concentration caused rapid filling of the whole GUV when low molecular weight fluorescent dextrans (Alexa-dextran 3000 (D3) or FITC-dextran 4000 (D4) with hydrodynamic radii of ~1.4 nm) were in the surrounding medium (Fig. 1*A*). The filling of each GUV was complete in minutes (Fig. 1*B*) and indicates transmembrane pore formation. The flux of high molecular weight fluorescent dextrans (Oregon Green- or FITC-labeled dextran 70,000 (D70) with hydrodynamic radii of 6 nm) into GUVs was insignificant even with prolonged incubation for 45 min (Fig. 1, *A* and *C*). No further changes in the number of permeabilized GUVs were observed with prolonged incubation for any of the probes tested. The *open black circles* in Fig. 1*C* thus represent the final proportion of permeabilized GUVs. The influx of the intermediate probe (Alexa- or FITC-labeled dextran 10,000 (D10) with hydrodynamic radius of ~1.8 nm) was slower than that of the small probe (Fig. 1*B*), but nevertheless, approximately half of the vesicles were filled with this probe after 45 min. After that time, we did not observe any further changes in the number of permeabilized GUVs indicating that 45 min is a sufficient time period for formation of functional PFN pores on GUV membranes and for passage of D10 into the interior of permeabilized GUVs. These results clearly show that medium size probes, such as D10, which have a similar size to granzyme B, can also pass through the pores, but the physiological relevance of this direct transfer is questionable because diffusion of such molecules through the pore is relatively slow (Fig. 1, *B* and *C*). When both small and intermediate probes were used, we could clearly discriminate vesicles that were filled with either probe or only the small one (Fig. 1*D*), indicating that some of the pores formed on the GUV membrane were not of sufficient size to allow the passage of the intermediate probe.

PFN Forms Heterogeneous Pores in Planar Lipid Membranes—We independently assessed the single pore sizes of native human PFN by determining the conductance distribution of pores in planar lipid membranes. The existing PLM studies that used cytotoxic granule extracts or isolated PFN indicated that PFN pore formation is dependent on the pres-

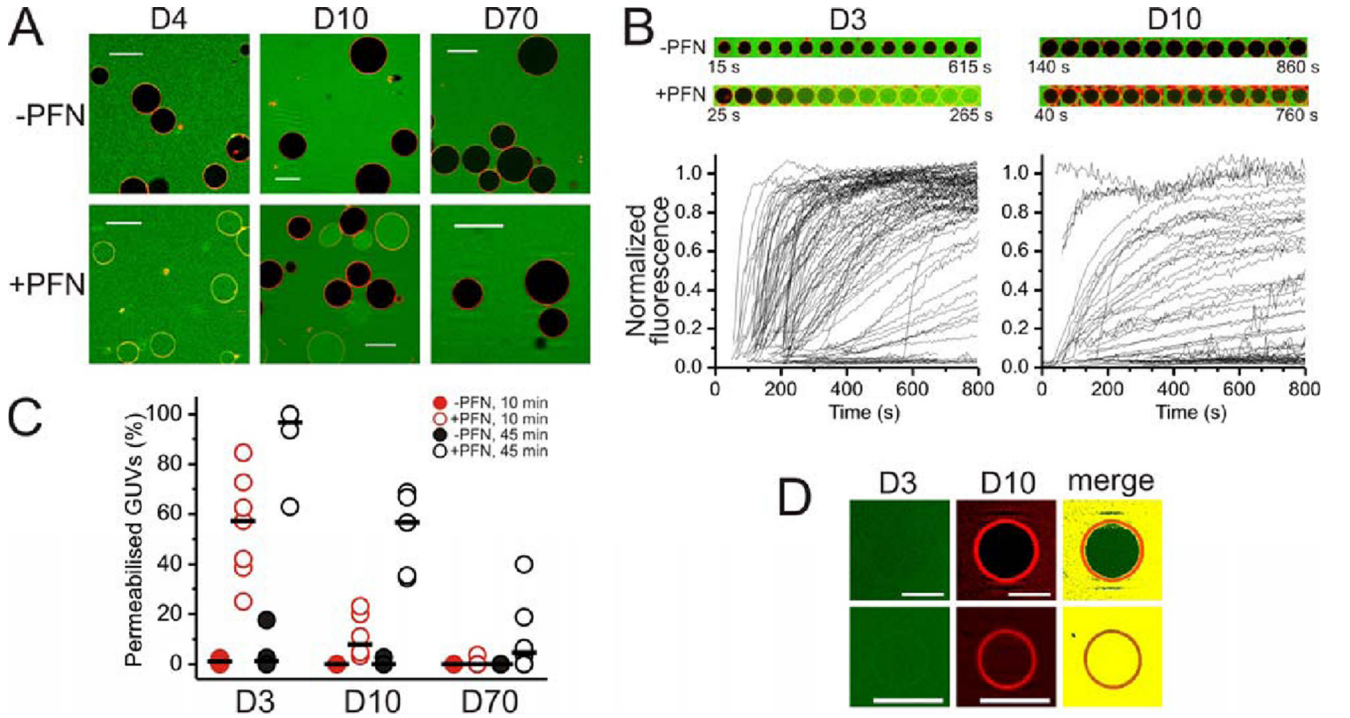

FIGURE 1. **GUVs are rapidly permeabilized in the presence of PFN.** *A,* GUVs in the absence or presence of 48 nM PFN and different fluorescent probes after 45 min incubation at room temperature. *Scale bar,* 20 μm. *B,* time courses of GUVs filling with D3 and D10 in the presence and absence of 12 nM PFN. Time courses of GUVs filling of 89 and 55 vesicles are shown for D3 and D10, respectively. *C,* proportion of permeabilized GUVs for different probes after 10 or 45 min of incubation. Each data point represents an independent experiment, and the median is shown by the *black line*. In total, 4–8 independent experiments were performed with 106–211 GUVs analyzed. *D,* example of two GUVs imaged after 45 min of incubation with 12 nM PFN, D3, and D10. The membrane contained also rDHPE. The *upper row* shows a GUV which was permeabilized only for D3, although the one presented in the *bottom row* of images was permeable to both probes.

ence of calcium ions and that pores were heterogeneous in size (20, 32–35). By using homogeneous PFN (22), supplemented with Ca^{2+}, we confirmed these findings in DPhPC planar membranes. In the control experiment performed in the absence of Ca^{2+}, we did not observe any PFN activity over a 30-min period (Fig. 2), although the concentration of PFN was ~10-fold higher than in other experiments where we observed insertion of PFN into PLM (Fig. 3). Soon after addition of 5 mM $CaCl_2$, we observed an increase in conductance in agreement with Ca^{2+}-dependent formation of pores by PFN (Fig. 2, *point iii*). Pores were usually formed 1–5 min after 0.5 nM PFN addition to a stable bilayer in the presence of Ca^{2+} (Fig. 3). In the next step, we analyzed PFN pore properties in detail, also focusing on the effect of phosphatidylcholines with mono- (POPC) or di-unsaturated acyl chains (DOPC) and the incorporation of CHO on pore conductance.

The addition of nM PFN to planar lipid bilayers composed of various lipids causes an increase in transmembrane current within 30–300 s (Fig. 3). Within a few minutes after the appearance of the first pore, the total ionic current reached a plateau, which was stable regardless of the polarity of the applied voltage (see below and Fig. 4*B*). Because PFN readily formed pores in all tested lipid compositions, a preferential lipid requirement was not apparent (Fig. 3). Nevertheless, substantial differences in current traces were noted, consistent with the gradual opening of individual pores as well as well resolved stepwise openings (Fig. 3). Gradual current increases with nonresolved step-like jumps were observed on DPhPC and DOPC membranes and where 20% of CHO was

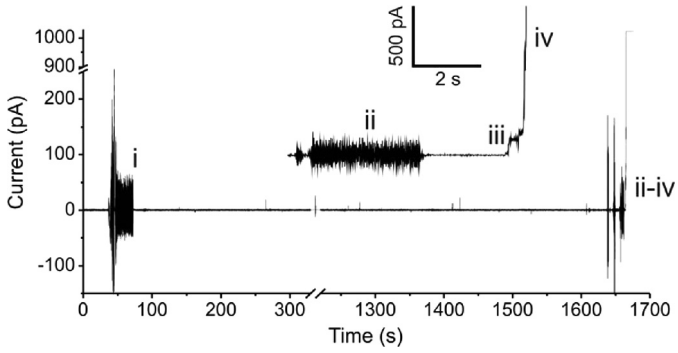

FIGURE 2. **Calcium-dependent activity of purified human perforin.** Pore formation is absolutely dependent on the presence of calcium ions. Addition of 4.7 nM PFN (~10-fold higher concentration than in other experiments reported here) to a stable bilayer composed of DPhPC in buffer containing 100 μM $CaCl_2$, and 1 mM EDTA did not give a pore (*i*); 5 mM $CaCl_2$ was added ~27 min after PFN addition (*ii*) causing the formation of PFN pore (*iii*) and subsequently the rupture of the membrane (*iv*). The current was measured at a constant voltage of +40 mV.

added to DOPC membranes (see Fig. 3, *inset i,* for the representative trace on DPhPC membrane). Gradual increases of this kind were not seen in similar experiments with CDCs. In these experiments, it was difficult to resolve individual pore apertures, and the pore size estimate was obtained from results of single channel experiments (see below). In contrast, POPC membranes containing various concentrations of CHO enabled stepwise increases in currents, which were very clear at high CHO concentrations. For example, the opening of individual pores could be easily discriminated with a mem-

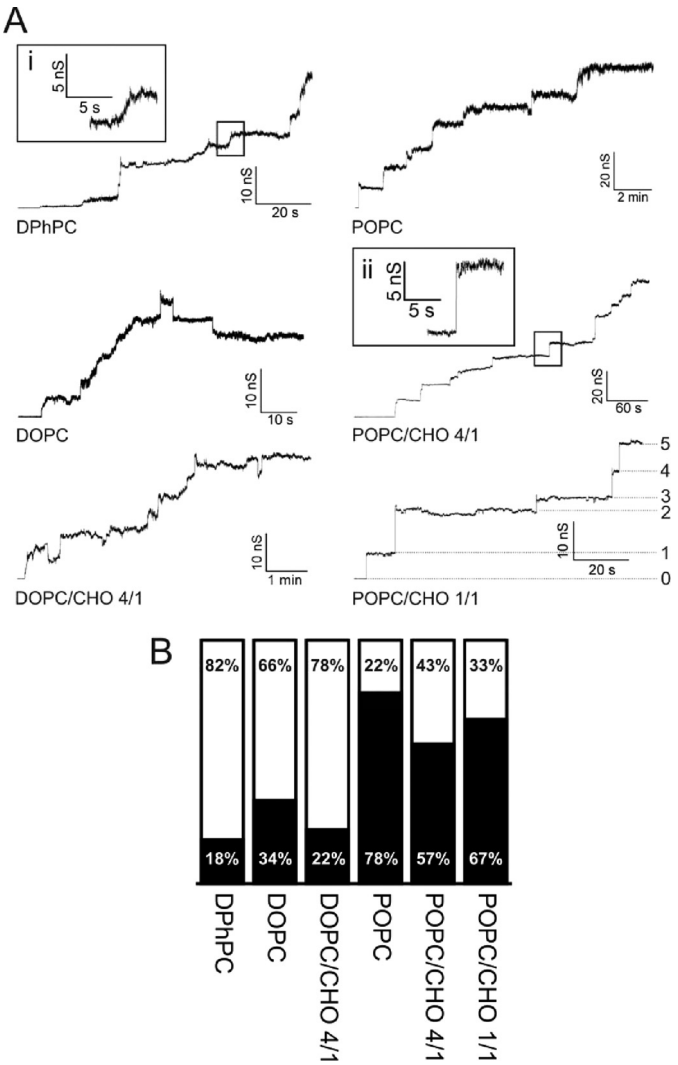

FIGURE 3. **PFN pores on PLM composed of various lipids.** *A,* representative conductance traces of at least four independent multichannel experiments are shown for each lipid composition tested. PFN was added to the *cis* side at 0.5–1.1 nM concentration. Pores started to form 30–300 s after addition of PFN. Two different types of pore openings, gradual (*panel i*) and discrete (*panel ii*), are magnified. Individual pores are marked on POPC/CHO 1:1 membrane. *B,* PFN pores assemble and insert in a gradual or discrete manner. We show the percentage of gradual or discrete openings of PFN pores on PLM composed of DPhPC (86 pores analyzed), DOPC (38 pores), DOPC/CHO 4:1 (24 pores), POPC (37 pores), POPC/CHO 4/:1 (88 pores), and POPC/CHO 1:1 (61 pores). *Unshaded* regions denote gradual openings and *shaded* regions discrete openings.

brane consisting of POPC/CHO, 1:1 (mol/mol) (see Fig. 3, *inset ii,* for a representative trace).

Conductance increments were variable in amplitude, ranging from 0.15 to 21 nS (Fig. 4). The observed distribution of single channel conductances is slightly larger than reported previously (20). This broad distribution strongly suggests the co-presence of pores, ranging in size from 2 to 22 nm in diameter (as estimated from Equation 3). It appears that larger pores predominated in membranes with lipid compositions that favor opening of discrete pores, *i.e.* POPC, POPC/CHO (4:1), and POPC/CHO (1:1) membranes lacked pores that displayed conductances <1 nS. On the other hand, smaller pores were frequent on the bilayers composed of DPhPC, DOPC, and DOPC/CHO (4:1).

We also noted that PFN pores that assembled on various membranes possessed distinct levels of current noise (Fig. 4). Small pores (G <2 nS) were always associated with high noise and exhibited a generally unstable character. The current traces were often associated with sudden stepwise increases or decreases and sometimes they completely closed (see *pores 1* and *2* in Fig. 4*A*). Larger pores (G >2 nS) possessed slightly lower noise (*pores 3* and *4* in Fig. 4*A*); however, some were associated with a very low noise current trace (*pores 5* and *6* in Fig. 4*A*). These pores possessed conductances between 5 and 14 nS and were stable for up to 1 h. The calculated diameter of such low noise pores was 11–18 nm corresponding to ring-shaped pores observed by electron microscopy (13–15).

By arbitrarily clustering pores into three groups, small high noise (G <2 nS) and large (G >2 nS) with either high or low noise, we also determined some of the properties of pores on the DPhPC bilayer. As observed by the linear current-voltage relationship for the three groups, PFN pores were not voltage-dependent. Minor rectification at negative voltages was observed only for the small pores (Fig. 4, *B* and *C*). As expected for large aqueous transmembrane channels, PFN pores were poorly selective. However, the selectivity of small pores was slightly anionic, although larger pores displayed a slightly cationic preference regardless of their noise level (Fig. 4*D*). The pneumococcal CDC, pneumolysin, similarly exhibits a wide range of conductances, where small pores are cation-selective, although large pores are unselective (36).

We also noted that the formation and stability of large pores were highly dynamic. For example, more than 80% of the openings of larger pores with low noise were preceded by smaller increases in current displaying high noise (Figs. 4, *pore 5,* and 5*A*). In most instances, the noise stabilized (Fig. 5*B*) and then remained constant for up to 1 h. On rare occasions, the stable low noise pore (possibly a double-arc pore, see Fig. 4, *pore 4*, and under "Discussion") appeared to undergo disassembly causing a sudden reduction in current associated with an increase in noise (Fig. 5*B*). When the current spontaneously returned to the previous level, the noise also returned to the former level suggesting restoration of a purely proteinaceous pore. The fact that the same conductance is found in a membrane before and after a period of lower, noisier conductance suggests that a single pore has broken up into a more disordered arrangement before reforming an ordered one. This is in striking distinction to the CDCs where pores open once and do not fluctuate in this manner.

Altogether, the GUVs and PLM data are in agreement with the published literature that describes perforin-induced membrane pores in the presence of Ca^{2+} ions (16, 19, 20, 37, 38). The purity of the PFN used (see "Experimental Procedures") (22) and the absence of a calcium-independent pore activity such as that of granulysin (39) (Fig. 2) indicate that the heterogeneous population of functional pores are the product of PFN activity alone. A heterogeneous pore size has been observed in the related CDCs also and has been explained by the existence of pores formed by arcs as well as rings of protein (9). If arcs do form then the conducting channel would be defined by the protein on one side and a lipidic boundary, presumably in a toroidal arrangement, on the other (9). Ap-

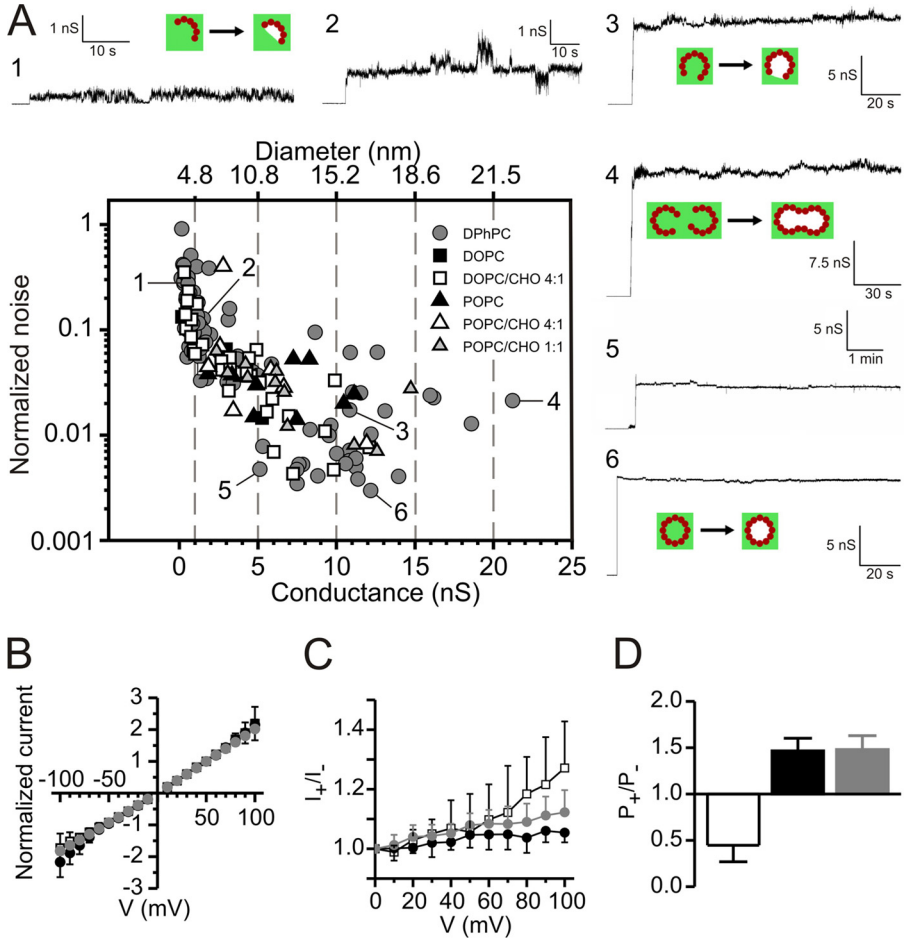

FIGURE 4. **Conductance traces reveal diverse mechanisms of PFN pore formation.** *A,* graph showing that PFN pores exhibit a wide range of conductances and current noise values. The calculated values for the pore diameter are shown *above* the graph, and representative pore traces are labeled by *numbers* in the graph and depicted around the graph. The schematic representations show possible mechanisms of pore formation (*green* = lipid, *red* = PFN, and *white* = pore) as also discussed in the text. Presented *pores 1–6* were observed on DPhPC membrane. *B–D,* PFN pore properties. PFN pores were arbitrarily divided into three groups on the basis on their conductances and noise levels: small pores with high noise (*black empty squares*), large pores with high noise (*gray circles*), and large pores with low noise (*black circles*). *B,* current-voltage relationship. Means of 4–10 single channel experiments ± S.D. are presented. Current values were normalized by dividing by current values gathered at 50 mV. *C,* ratio between positive and negative current (I_+/I_-) as a function of the applied potential, data taken from *B*. *D,* pore selectivity. Means of 3–6 single channel experiments ± S.D. are presented. Electrophysiological properties were examined on PLM composed of DPhPC.

parent pores formed by PFN oligomeric arcs (as opposed to rings) have been observed (15, 16, 40), which supports the idea that they provide an explanation for the variable pore sizes we detect.

PFN Forms Heterogeneous Pores on Large Unilamellar Vesicles—To enable us to visualize the interaction of PFN with membranes in molecular detail, we switched to an LUV-based system in which cryo-EM of the membrane with bound protein is viable. On addition of PFN to LUVs, we observed pore-like structures with a range of sizes and morphologies (Fig. 6*A*). By taking 128 images of membrane-bound PFN oligomers, we were able to define two distinct conformations for PFN bound to membranes, one of which is the pore-forming state and the other of which appears to be a pre-pore state.

It is apparent from the raw images (Fig. 6*A*) that substantial variability is observed in the size and planarity of PFN oligomers. The pore diameters varied from 10 to 25 nm (Fig. 6*B*), but the average of all the images clearly shows a pore-like structure (Fig. 6*C*). The size distribution (Fig. 6*B*) resembles the distribution of single channel conductances (Fig. 4*A*) but lacking small pores. We suspect that PFN pores smaller than 10 nm are too small to be detected by cryo-EM. This range of sizes is wider than described previously (20) but in line with pores formed by arcs and possibly between two arcs (9, 17). To seek a more focused classification, we limited our assessment of image similarity to one side of the pore-like oligomeric structure (Fig. 6*C*, *boxed*, and results are shown in Fig. 6*D*). This allowed us to view two clearly different PFN structures bound to the membrane surface as follows: one in which the molecule has a comma-like shape (19 images in class) and its head is cocked back, and the other in which the molecule is more linear and seems to stand upright above the membrane (22 images in class). As shown, focusing our classification on one side of the oligomer not only sharpened the clarity with which we could see the PFN subunit profile, but it also smeared out the other half of the structure. This underscores the diversity of pore diameters in the images (supplemental Fig. 2) and has allowed us to pinpoint two different membrane-bound states of PFN. It is notable that the comma-shaped conformation is associated with an unbroken lipid

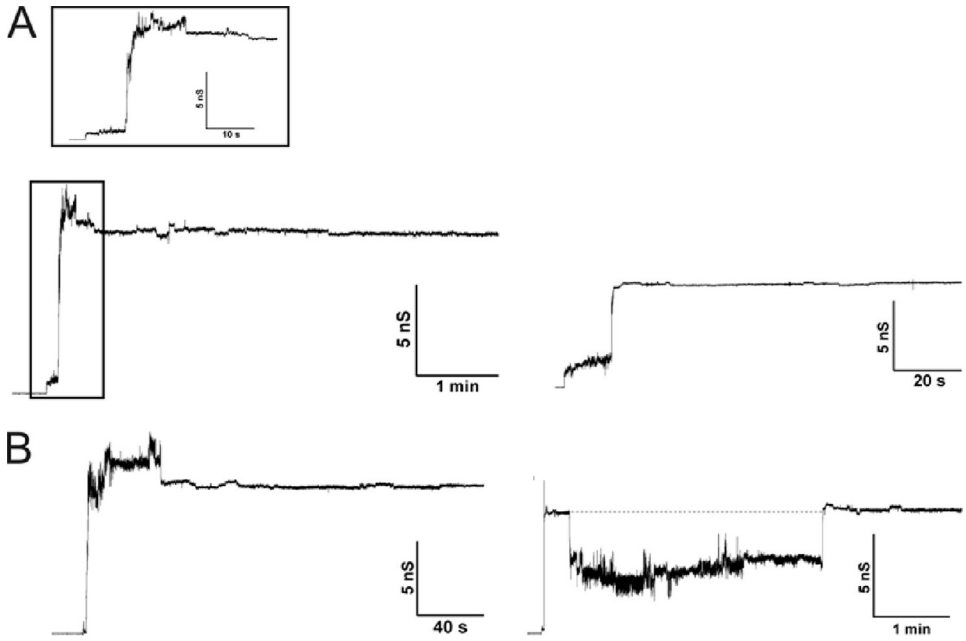

FIGURE 5. **Several examples of pores exhibiting variable noise.** *A,* openings of large pores were frequently preceded by smaller increases in conductance. Here, we show two typical examples as follows: on the *left* (expanded view above) the presence of a noisy low conductance pore before the sudden opening of an initially noisy and then noise-free pore, and on the *right* a more prolonged noisy and gradually opening pore prior to the appearance of a large pore with low noise. *B,* after initial high noise in many cases, the pore stabilized, remaining stable for up to an hour. We also observed the apparent interconversion of a noise-free large conductance and a noisy lower conductance pore.

membrane (it is pre-pore), but the upright conformation is associated with a hole through the membrane, the PFN pore. A subset of 34 of the images, which aligned with respect to one side of the oligomer, did classify together to show a symmetrical pore-like structure (Fig. 6*E*), which would correspond to larger pores (conductances 11–14 nS) in Fig. 4*A*. This demonstrates that some symmetrical structures of this kind exist because we avoided the possible effect of model bias by only aligning one side of the pore data to a reference image, yet we considered both sides in statistical analysis of image features to produce the average shown in Fig. 6*E*. Even so, alignment and classification on the basis of one side of the oligomer alone produced the best images of PFN bound to the membrane (Fig. 6*F*). Surface rendering of these by application of rotational symmetry (Fig. 6*G*) permitted the fitting of homology models of the PFN MACPF, EGF, and C2 domains (supplemental Fig. 1*A*), showing the dimensions of the pore match those expected for the molecule. As is also the case with CDCs, the comma-shaped (pre-pore) state matches better the MACPF domain shape than the upright (pore) state (9, 12, 41). This is consistent with what is known about the mechanism of MACPF/CDC superfamily proteins, because it suggests the refolding and extension of the pore-forming MACPF/CDC helical regions that insert into the membrane (12, 42–44) on PFN pre-pore-to-pore transition (supplemental Fig. 1).

DISCUSSION

Two models exist currently to explain the protein delivery function of PFN. The first involves formation of stable, albeit transiently functional, plasma membrane pores that allow the direct transfer of granzymes into the target cell (3, 32). This model is based primarily on visualization of pore-like structures on the membranes of target cells (16, 32, 40). In this study, we show that native human perforin forms heterogeneous pores on lipid membranes, and cryo-EM for the first time enabled monitoring of a pre-pore intermediate, which sits atop an unperturbed membrane. Although heterogeneity was noted before (20), the use of single-channel PLM experiments and cryo-EM indicate that it is much larger than thought previously. Larger pores are most likely fully assembled ring-shaped pores, in agreement with the dimensions of the pore shown on Fig. 6*E*, and those larger than the ring are perhaps two fused arcs (9, 17). Smaller pores are in our opinion the incomplete but nevertheless functional arc-shaped pores, which have been postulated for cholesterol-dependent cytolysins also.

Several models of pore formation exist for the related CDCs (9, 45), where complete oligomerization of monomers into the pre-pore was shown to occur prior to pore formation for perfringolysin O (43). The pre-pore complex inserts into the membrane in a single step, and discrete stepwise openings were indeed observed in a planar lipid bilayer setup (46). On the other hand, CDC oligomers are predicted to form incomplete arcs that are supposed to be functional. Arcs are viewed as transmembrane pores lined by a protein oligomer on one side and lipids on the other (9, 45, 47). Previously, we proposed a model in which the nature of the pore depends on the local concentration of monomer such that limiting levels predispose to pore formation by arcs rather than rings (9). Thus, depending on such variables as protein concentration and the lipid composition of the membrane, functional transmembrane arcs, double-arc pores, or fully assembled ring-shaped pores may be formed by CDC oligomers. Some of the electrophysiological data are in agreement with this model. For ex-

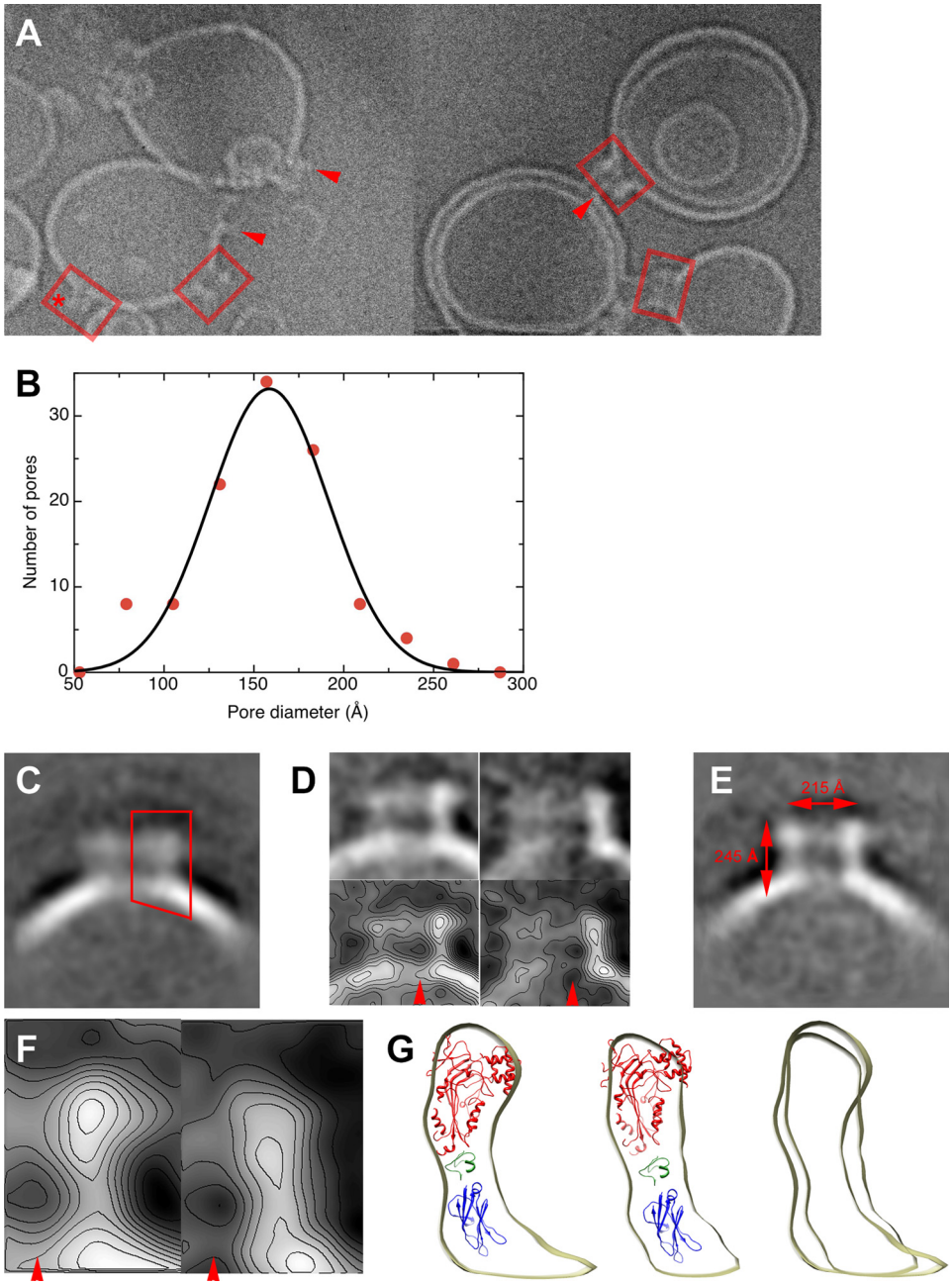

FIGURE 6. **Molecular details of pores formed on LUVs.** *A,* examples of cryo-EM images of PFN interacting with LUVs. Membrane-bound PFN oligomers are *boxed*, and a particularly narrow oligomer has an *asterisk*, and other superstructures are marked with *arrowheads*. *B,* distribution of pore and pre-pore diameters observed with no attempt to distinguish them. *C,* class average of 128 images of PFN bound to LUVs. *D,* image classification based on the right-hand side only of each data image (as *boxed* in *C*). Representative class averages and equivalent contour plots are shown. *Left,* comma shaped with intact membrane. *Right,* more upright, pore-associated (*arrowheads*). *E,* class average of data aligned to the *right-hand side* of the membrane-bound oligomer only (as in *C*) but classified on the whole structure. *F,* class average contour plots of iteratively aligned data with respect to one side only for pre-pore and pore conformations (*arrowheads*). *G,* fitting of the two different conformations of PFN with homology models of the MACPF (*red*), EGF (*green*), and C2 (*blue*) domains of PFN (see supplemental Fig. 1*A*). On the *right*, pre-pore and pore densities are overlaid for comparison.

ample, it was shown that pneumolysin generates multiple conductance pores in the membranes of nucleated cells (48). Similarly, planar lipid bilayer experiments of a CDC from *Bacillus sphaericus* showed gradual as well as stepwise increases (49). The electrophysiological data reported here agree with these possibilities suggesting that PFN may also exist in different pore states.

The current traces (Fig. 3) and the variability in the pore size and noise level (Fig. 4) not only suggest the existence of multiple PFN pore states but also indicate that distinct mechanisms are responsible for their formation. Current traces with high noise indicate small pores (Fig. 4, *pores 1* and *2*) or large transmembrane arcs (Fig. 4, *pores 3* and *4*,). The inherent noise of such pores may be due to the less rigid structure of arcs and the presence of flexible and dynamic lipids as part of the actual pore boundary. Extremely large increases in current are probably caused by formation of double-arc pores by fusion of two arcs within the membrane (Fig. 4, *pore 4*). Fully

assembled pores appear to form by maturation of previously inserted arcs to a final stable ring-shaped proteinaceous pore (Fig. 5*A*), but it can also be formed instantaneously by the insertion of a fully assembled ring-shaped pre-pore complex into the membrane (Fig. 4, *pores 5* and *6*). Thus, our results are in accordance with both the "growing arcs" and the "pre-pore to pore transition" model, where composition of lipids and local protein concentration favors one or the other pathway. The sliding increase in conductance seen in some pores (Figs. 3*A* and 5*B*) could be explained by the movement of lipids away from PFN on the membrane, and this could be due to either a direct effect of the pre-pore state or an inserted arc of PFN. Another explanation for the sliding increase in conductance would be the addition of further PFN molecules, either already formed into other oligomeric arcs or from a remaining pool of monomeric protein.

It is generally accepted that the physical state of the plasma membrane plays an important role in the functioning of membrane proteins (50) and can have, in the case of pore-forming peptides and proteins, important consequences on the latter steps in the pore-forming process (51–53). One crucial parameter in protein-lipid interactions is the ordering of lipid acyl chains. The structure of headgroups used in our PLM experiments was identical, but the acyl chains differed with ordering that decreased as follows: POPC > DOPC > DPhPC (54). Our results clearly show that the ordering of the acyl chains influences the mechanism of pore formation, which agrees very well with the known dependence of pore formation on temperature in MACPF/CDC proteins (10, 11) and the idea that pore formation is a kinetically governed event (9). Less ordered acyl chains (DPhPC and DOPC) allow the prompt insertion of PFN oligomers, which then may expand by addition of monomers or smaller oligomers or the effect of the membrane-inserted protein on the membrane lipid arrangement. This possibility is manifested in gradual increases of current and occurrence of small pores (Figs. 3 and 4). Lipids with more ordered acyl chains (*e.g.* POPC) minimize the inadvertent insertion of oligomers leading to the preferential formation of a full ring-shaped pre-pore on the membrane surface and thereby a pore. In the next step, the whole complex (complete or nearly completely assembled pre-pore) inserts into the bilayer resulting in a discrete jump in the conductance of such pores (Fig. 4, *pores 3–6*). Although the presence of CHO did not appear to affect the mechanism of pore formation (Fig. 3*B*), the stepwise current increases were clearest for membranes with the highest CHO content (Fig. 3) with most pores having low noise (Fig. 4). This agrees with the ability of CHO to promote protein oligomerization (55, 56) and order acyl chains of lipids (54).

In summary, by using different model systems with diverse membrane curvature (PLM, LUVs, and GUVs), we show that PFN forms pores that are more heterogeneous than anticipated. In addition to large, ring-shaped pores previously discovered by electron microscopy, we show here that PFN also forms smaller, less stable pores, presumably by lipids closing the gap between the two ends of a PFN arc. The observation of two membrane-bound PFN conformations, one associated with a pore and the other not, indicates that a pre-pore oligomer as well as a pore oligomer can form. However, our data provide evidence for the expansion of pore size after pore formation, which is lacking for CDCs, and therefore shows a difference in mechanism. This is likely to be further complicated by consideration of the mechanisms by which PFN-related proteins facilitate phenotypes such as *Plasmodium* gliding through cells (57) and, separately, invasion of insect midgut cells (58, 59). Indeed, the common CDC/MACPF fold seems to have been selected for its membrane-focused activity but not for only one kind of membrane permeabilization event.

Acknowledgments—We thank to Dr. Janja Majhenc and Vesna Arrigler for the help with the GUV electroformation and Dr. Mojca Benčina for the help with the confocal microscopy.

REFERENCES

1. Pipkin, M. E., and Lieberman, J. (2007) *Curr. Opin. Immunol.* **19,** 301–308
2. Voskoboinik, I., Smyth, M. J., and Trapani, J. A. (2006) *Nat. Rev. Immunol.* **6,** 940–952
3. Metkar, S. S., Wang, B., Aguilar-Santelises, M., Raja, S. M., Uhlin-Hansen, L., Podack, E., Trapani, J. A., and Froelich, C. J. (2002) *Immunity* **16,** 417–428
4. Uellner, R., Zvelebil, M. J., Hopkins, J., Jones, J., MacDougall, L. K., Morgan, B. P., Podack, E., Waterfield, M. D., and Griffiths, G. M. (1997) *EMBO J.* **16,** 7287–7296
5. Voskoboinik, I., Thia, M. C., Fletcher, J., Ciccone, A., Browne, K., Smyth, M. J., and Trapani, J. A. (2005) *J. Biol. Chem.* **280,** 8426–8434
6. Hadders, M. A., Beringer, D. X., and Gros, P. (2007) *Science* **317,** 1552–1554
7. Rosado, C. J., Kondos, S., Bull, T. E., Kuiper, M. J., Law, R. H., Buckle, A. M., Voskoboinik, I., Bird, P. I., Trapani, J. A., Whisstock, J. C., and Dunstone, M. A. (2008) *Cell. Microbiol.* **10,** 1765–1774
8. Anderluh, G., and Lakey, J. H. (2008) *Trends Biochem. Sci.* **33,** 482–490
9. Gilbert, R. J. (2005) *Structure* **13,** 1097–1106
10. Tweten, R. K. (2005) *Infect. Immun.* **73,** 6199–6209
11. Baran, K., Dunstone, M., Chia, J., Ciccone, A., Browne, K. A., Clarke, C. J., Lukoyanova, N., Saibil, H., Whisstock, J. C., Voskoboinik, I., and Trapani, J. A. (2009) *Immunity* **30,** 684–695
12. Tilley, S. J., Orlova, E. V., Gilbert, R. J., Andrew, P. W., and Saibil, H. R. (2005) *Cell* **121,** 247–256
13. Blumenthal, R., Millard, P. J., Henkart, M. P., Reynolds, C. W., and Henkart, P. A. (1984) *Proc. Natl. Acad. Sci. U.S.A.* **81,** 5551–5555
14. Masson, D., and Tschopp, J. (1985) *J. Biol. Chem.* **260,** 9069–9072
15. Young, J. D., Cohn, Z. A., and Podack, E. R. (1986) *Science* **233,** 184–190
16. Young, J. D., Hengartner, H., Podack, E. R., and Cohn, Z. A. (1986) *Cell* **44,** 849–859
17. Bhakdi, S., Tranum-Jensen, J., and Sziegoleit, A. (1985) *Infect. Immun.* **47,** 52–60
18. Bashford, C. L., Alder, G. M., Graham, J. M., Menestrina, G., and Pasternak, C. A. (1988) *J. Membr. Biol.* **103,** 79–94
19. Peters, R., Sauer, H., Tschopp, J., and Fritzsch, G. (1990) *EMBO J.* **9,** 2447–2451
20. Bashford, C. L., Menestrina, G., Henkart, P. A., and Pasternak, C. A. (1988) *J. Immunol.* **141,** 3965–3974
21. Sauer, H., Pratsch, L., Tschopp, J., Bhakdi, S., and Peters, R. (1991) *Biochim Biophys Acta* **1063,** 137–146
22. Froelich, C. J., Turbov, J., and Hanna, W. (1996) *Biochem. Biophys. Res. Commun.* **229,** 44–49
23. Peterlin, P., and Arrigler, V. (2008) *Colloids Surf.* **B64,** 77–87
24. Dalla Serra, M., and Menestrina, G. (2000) *Methods Mol. Biol.* **145,** 171–188
25. Mindell, J. A., and Grigorieff, N. (2003) *J. Struct. Biol.* **142,** 334–347
26. Ludtke, S. J., Baldwin, P. R., and Chiu, W. (1999) *J. Struct. Biol.* **128,**

82–97
27. van Heel, M., Harauz, G., Orlova, E. V., Schmidt, R., and Schatz, M. (1996) *J. Struct. Biol.* **116,** 17–24
28. Pettersen, E. F., Goddard, T. D., Huang, C. C., Couch, G. S., Greenblatt, D. M., Meng, E. C., and Ferrin, T. E. (2004) *J. Comp. Chem.* **25,** 1605–1612
29. Kelley, L. A., MacCallum, R. M., and Sternberg, M. J. (2000) *J. Mol. Biol.* **299,** 499–520
30. Bennett-Lovsey, R. M., Herbert, A. D., Sternberg, M. J., and Kelley, L. A. (2008) *Proteins* **70,** 611–625
31. Praper, T., Besenicar, M. P., Istinic, H., Podlesek, Z., Metkar, S. S., Froelich, C. J., and Anderluh, G. (2010) *Mol. Immunol.* **47,** 2492–2504
32. Podack, E. R., Young, J. D., and Cohn, Z. A. (1985) *Proc. Natl. Acad. Sci. U.S.A.* **82,** 8629–8633
33. Young, J. D., Leong, L. G., Liu, C. C., Damiano, A., and Cohn, Z. A. (1986) *Proc. Natl. Acad. Sci. U.S.A.* **83,** 5668–5672
34. Young, J. D., Nathan, C. F., Podack, E. R., Palladino, M. A., and Cohn, Z. A. (1986) *Proc. Natl. Acad. Sci. U.S.A.* **83,** 150–154
35. Young, J. D., Podack, E. R., and Cohn, Z. A. (1986) *J. Exp. Med.* **164,** 144–155
36. Korchev, Y. E., Bashford, C. L., and Pasternak, C. A. (1992) *J. Membr. Biol.* **127,** 195–203
37. Browne, K. A., Blink, E., Sutton, V. R., Froelich, C. J., Jans, D. A., and Trapani, J. A. (1999) *Mol. Cell. Biol.* **19,** 8604–8615
38. Podack, E. R., and Dennert, G. (1983) *Nature* **302,** 442–445
39. Stenger, S., Hanson, D. A., Teitelbaum, R., Dewan, P., Niazi, K. R., Froelich, C. J., Ganz, T., Thoma-Uszynski, S., Melián, A., Bogdan, C., Porcelli, S. A., Bloom, B. R., Krensky, A. M., and Modlin, R. L. (1998) *Science* **282,** 121–125
40. Young, L. H., Joag, S. V., Zheng, L. M., Lee, C. P., Lee, Y. S., and Young, J. D. (1990) *Lancet* **336,** 1019–1021
41. Gilbert, R. J., Jiménez, J. L., Chen, S., Tickle, I. J., Rossjohn, J., Parker, M., Andrew, P. W., and Saibil, H. R. (1999) *Cell* **97,** 647–655
42. Heuck, A. P., Tweten, R. K., and Johnson, A. E. (2003) *J. Biol. Chem.* **278,** 31218–31225
43. Shatursky, O., Heuck, A. P., Shepard, L. A., Rossjohn, J., Parker, M. W., Johnson, A. E., and Tweten, R. K. (1999) *Cell* **99,** 293–299
44. Heuck, A. P., Hotze, E. M., Tweten, R. K., and Johnson, A. E. (2000) *Mol. Cell* **6,** 1233–1242
45. Bayley, H. (1997) *Curr. Biol.* **7,** R763–R767
46. Shepard, L. A., Shatursky, O., Johnson, A. E., and Tweten, R. K. (2000) *Biochemistry* **39,** 10284–10293
47. Palmer, M., Harris, R., Freytag, C., Kehoe, M., Tranum-Jensen, J., and Bhakdi, S. (1998) *EMBO J.* **17,** 1598–1605
48. El-Rachkidy, R. G., Davies, N. W., and Andrew, P. W. (2008) *Biochem. Biophys. Res. Commun.* **368,** 786–792
49. From, C., Granum, P. E., and Hardy, S. P. (2008) *FEMS Microbiol. Lett.* **286,** 85–92
50. Findlay, H. E., and Booth, P. J. (2006) *Phys. Cond. Matter* **18,** S1281–S1291
51. Poklar, N., Fritz, J., Macek, P., Vesnaver, G., and Chalikian, T. V. (1999) *Biochemistry* **38,** 14999–15008
52. Yang, L., Harroun, T. A., Weiss, T. M., Ding, L., and Huang, H. W. (2001) *Biophys. J.* **81,** 1475–1485
53. Heller, W. T., He, K., Ludtke, S. J., Harroun, T. A., and Huang, H. W. (1997) *Biophys. J.* **73,** 239–244
54. Bakht, O., Pathak, P., and London, E. (2007) *Biophys. J.* **93,** 4307–4318
55. Chattopadhyay, K., Bhattacharyya, D., and Banerjee, K. K. (2002) *Eur. J. Biochem.* **269,** 4351–4358
56. Palmer, M. (2004) *FEMS Microbiol. Lett.* **238,** 281–289
57. Amino, R., Giovannini, D., Thiberge, S., Gueirard, P., Boisson, B., Dubremetz, J. F., Prévost, M. C., Ishino, T., Yuda, M., and Ménard, R. (2008) *Cell Host Microbe* **3,** 88–96
58. Ecker, A., Pinto, S. B., Baker, K. W., Kafatos, F. C., and Sinden, R. E. (2007) *Exp. Parasitol.* **116,** 504–508
59. Ecker, A., Bushell, E. S., Tewari, R., and Sinden, R. E. (2008) *Mol. Microbiol.* **70,** 209–220